Heliyon 10 (2024) e33200

Contents lists available at ScienceDirect

Heliyon

journal homepage: www.cell.com/heliyon

Research article

Analysis of cell death-related genes to evaluate the prognostic and immunotherapeutic value in bladder cancer

Mingde Gao [a,1], Haifeng Guo [a,1], Haifei Xu [a,1], Xiaoxia Jin [b], Yushan Liu [b], Zhigang Chen [a,**], Xiaolin Wang [a,*]

[a] Department of Urology, Affiliated Tumor Hospital of Nantong University & Nantong Tumor Hospital, Nantong 226300, China
[b] Department of Pathology, Affiliated Tumor Hospital of Nantong University & Nantong Tumor Hospital, Nantong 226300, China

ARTICLE INFO

Keywords:
Cell demise indicator
Prognosis
Immunotherapy
Bladder cancer
CHMP4C
GSDMB

ABSTRACT

To enhance therapeutic approaches, we created a distinctive pattern utilizing the cell demise indicator (CDI) to predict the effectiveness of immunotherapy in individuals with bladder carcinoma (BLCA). Hub prognostic CDIs were identified from the TCGA database using differential gene expression and survival analysis, encompassing 763 genes across 13 death modes. The subtype assessment was employed to evaluate the impact of these genes on the prognosis and immunotherapeutic outcomes in patients with BLCA. The LASSO regression method was used to identify significant CDIs, while Cox regression and nomogram analyses were conducted to explore the impact of CDIs on prognosis. CHMP4C and GSDMB were selected as the hub genes for the following research. Subsequently, These two central genes underwent further investigation to explore their association with immunotherapy, followed by an analysis of their potential regulatory network. Subtype analysis showed that these CDIs were significantly associated with the prognosis and immunotherapy of BLCA patients. The regulatory network in BLCA was evaluated through the establishment of the lncRNA XIST/NEAT1-CDIs-miR-146a-5p/miR-429 axis. Immunohistochemical analysis revealed a significant up-regulation of CHMP4C in bladder cancer tissues, which was strongly associated with an unfavorable prognosis for BLCA patients. Moreover, our findings provide compelling evidence that CHMP4C plays a pivotal role in promoting BLCA progression through the activation of the epithelial-mesenchymal transition (EMT) pathway. These findings highlight the negative impact of CHMP4C on BLCA patient prognosis, while also providing insights into the oncogenic mechanisms and immunotherapy in which CHMP4C may be involved.

Abbreviations: ACD, accidental cell death; RCD, regulatory cell death; BLCA, bladder cancer; CDI, cell demise indicator; DEGs, differential expressed genes; TIME, tumor immune microenvironment; ICB, immune checkpoint blockade; TIDE, Tumor Immune Dysfunction and Exclusion; EMT, epithelial–mesenchymal transition; GSEA, Gene Set Enrichment Analysis.

* Corresponding author. Department of Urology, Affiliated Tumor Hospital of Nantong University & Nantong Tumor Hospital, No. 30 Tongyang Bei Road, Tongzhou District, Nantong 226300, China.

** Corresponding author. Department of Urology, Affiliated Tumor Hospital of Nantong University & Nantong Tumor Hospital, No. 30 Tongyang Bei Road, Tongzhou District, Nantong 226300, China.

E-mail addresses: ntczg@163.com (Z. Chen), cxhwyc2010@163.com (X. Wang).

[1] These authors contributed equally to this work.

https://doi.org/10.1016/j.heliyon.2024.e33200
Received 8 January 2024; Received in revised form 11 June 2024; Accepted 17 June 2024
Available online 17 June 2024
2405-8440/© 2024 Published by Elsevier Ltd. This is an open access article under the CC BY-NC-ND license (http://creativecommons.org/licenses/by-nc-nd/4.0/).

1. Introduction

Comprehensively studying all modes of cell death could enhance our understanding of how tumor cells evade death. Both normal and tumor cells experience two conditions: survival and death. We hope that normal cells will survive while abnormal cells, such as tumor cells, will die. Therefore, the investigation of tumor cell death was of paramount importance in safeguarding human well-being. Accidental cell death (ACD) and regulated cell death (RCD) are the two categories of cell demise. ACD refers to uncontrolled cell death, while RCD involves controlled methods of cell death [1]. In this research, we studied 13 modes of cell death: apoptosis [2], necroptosis [2], pyroptosis [3], ferroptosis [4], entotic cell death [5], netotic cell death [5,6], parthanatos [5], lysosome-dependent cell death [5], autophagy [2], immunogenic cell death [7], alkaliptosis [8,9], oxeiptosis [10–12] and cuproptosis [13].

Globally, bladder cancer (BLCA) was one of the top 10 leading cancers, with approximately 549,000 new diagnoses and 200,000 fatalities in 2018 [14]. BLCA faced a continuous risk of recurrence and progression that can ultimately lead to patient death [15]. In the past few decades, traditional treatments for BLCA have included surgical resection, intravesical perfusion, systemic chemotherapy, and radiotherapy. Ongoing advancements in tumor microenvironment and immunotherapy research are being complemented by studies on sequencing and genetic expression, which have unveiled a plethora of DNA, RNA, and protein biomarkers in BLCA that have gained significant popularity in recent years [16,17]. Nevertheless, the outlook for individuals with BLCA remains dissatisfactory. Despite numerous studies conducted on BLCA, the overall incidence and mortality rates of BLCA remained unchanged in the past 20 years [18,19]. Therefore, it is urgent for us to construct new prognostic models and identify therapeutic targets for BLCA.

A pan-tumor study, which included apoptosis, autophagy, ferroptosis, necroptosis and pyroptosis, demonstrated a significant association between cell death and cancer prognosis as well as the tumor microenvironment [20]. In the previous study by Xu et al., the effects of apoptosis, ferroptosis, and necrosis on the prognosis and immunotherapy of BLCA were proven [21]. Additionally, Zhang et al. published a paper on pan-programmed cell death in BLCA which involved six modes of cell death: apoptosis, autophagy, cuproptosis, ferroptosis, necroptosis and pyroptosis. Their model's features were demonstrated to improve the accuracy of bladder cancer prognosis prediction [22]. In summary, we observed an association between BLCA and RCD, although the precise mechanism of cell death underlying this relationship remains elusive. Notably, BLCA did not investigate antotic cell death, netotic cell death, lysosome-dependent cell death, alkaliptosis, or oxeiptosis. Hence, a cell demise indicator (CDI) was formulated to evaluate the outlook and immunotherapy in individuals diagnosed with BLCA (Fig. 1).

2. Materials and methods

2.1. Selection and application of database

We obtained the RNA sequencing (RNA-seq) data and accompanying clinical information for BLCA from the Genomic Data Commons (GDC) data portal (TCGA), which is located at https//portal.gdc.cancer.gov/. After removing six duplicate tumor samples during data processing, there were a total of 433 BLCA samples combined, consisting of 408 tumor samples and 19 normal samples. Due to the notable distinction between tumor and normal samples, we obtained data from 21 bladder samples considered as normal from the GTEx V8 release version (https://gtexportal.org/home/datasets).

2.2. Identification of 12 prognostic genes

We confirmed 13 modes of death and identified 763 genes by searching previous studies or public databases (Supplementary Table 1). The limma R package was utilized to identify differentially expressed genes (DEGs) among the 763 CDIs that were identified, considering a P value < 0.05 and fold change >2. Prognosis evaluation was conducted using Kaplan-Meier (KM) survival analysis.

2.3. Subtype analysis

The consistency analysis was conducted using the R package called 'ConsensusClusterPlus'. ClusterAlg 'hc' with innerLinkage 'ward.D2' was used to draw 100 times from the 80 % of the total samples, with a maximum of 6 clusters. The R software was utilized to analyze the mRNA that was expressed differentially, employing the limma package. The threshold for the differential expression of mRNAs was defined as having an Adjusted P value less than 0.05 and a Log 2(Fold Change) greater than 1 or less than −1. Moreover, the ClusterProfiler package (3.18.0 version) was utilized in R to examine the GO function of potential targets and enhance the KEGG pathway. The boxplot was drawn using the R package called 'ggplot 2'. We obtained and visualized the mutation data using the maftools package in the R software. We utilized immuneeconv, an R software bundle that incorporated three state-of-the-art algorithms: TIMER, xCell, and CIBERSORT. To evaluate the immunological connection of the CDIs and anticipate the potential reaction to immune checkpoint blocking therapy (ICB), the Tumor Immune Dysfunction and Exclusion (TIDE) algorithm was utilized to extract the expression values of the 8 genes relevant to immune checkpoints.

2.4. Construction of a new prognostic model

The R software package 'glmnet' was used to perform LASSO analysis. Based on the findings from the LASSO regression analysis, a new risk score was formulated, and individuals diagnosed with BLCA were categorized into high-risk and low-risk groups based on the median threshold. The KM curve provided P-values and hazard ratios (HRs) along with 95 % confidence intervals (CIs) through log-

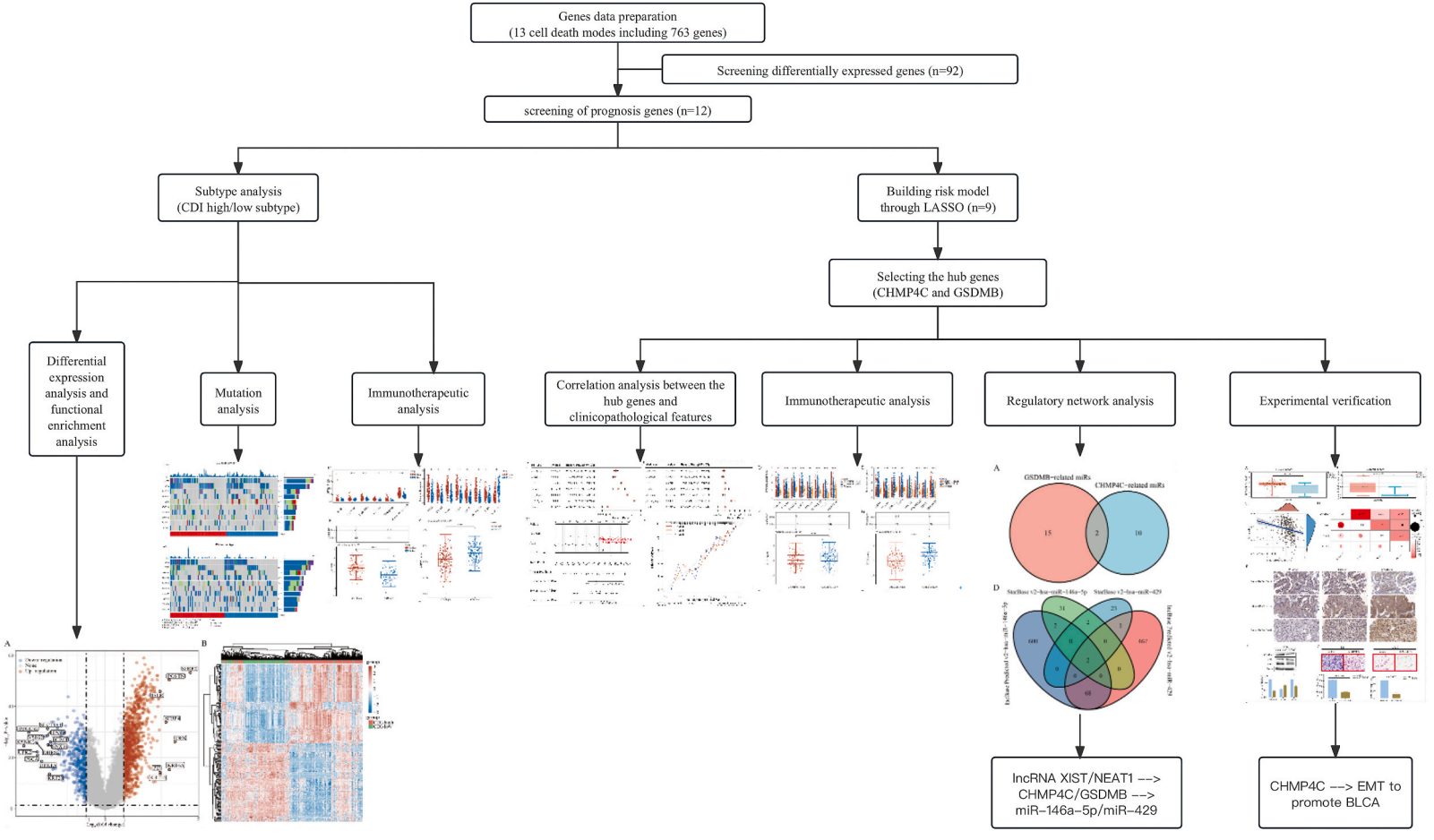

Fig. 1. Flow chart. The full text was displayed in the flow chart.

rank tests and univariate Cox proportional hazards regression. To assess the forecast accuracy of the risk score, the R software package called 'timeROC' was employed. Riskscore = (−0.1668) * NTF3 + (0.0227) * CRYAB + (0.0219) * HSPB8 + (0.0082) * DCN + (−0.0762) * CHMP4C + (0.0025) * NGF + (0.0712) * TRIB3 + (0.0677) * DAPL1 + (−0.2182) * GSDMB.

2.5. Identification and immune relevance of the hub CDIs

Based on the weight of all death genes, GSDMB and CHMP4C were selected as the next research targets. The R software package "forestplot" was used to generate a forest plot displaying the P value, HR, and 95 % CI of each variable. Using the outcomes of multivariate Cox proportional hazards analysis, a nomogram was created to forecast the overall survival (OS) for 1, 3, and 5 years. The R software package "pheatmap" was used to display the correlation analysis between the hub CDIs and the six immune cells. The R software package "estimate" was utilized to estimate the relationship between the 2 hub genes and the 3 immune scores (ImmuneScore, StromalScore, and ESTIMATEScore), respectively.

2.6. Construction of competing endogenous RNA (ceRNA) network and GSEA for the CDIs

To further explore the possible mechanisms of hub CDIs in BLCA, we predicted the upstream and downstream regions of CHMP4C and GSDMB. To assess miRNAs linked to these CDIs, we employed the miRTarBase and TarBase V.8, which are databases containing experimentally validated microRNA-target interactions. StarBase v2.0 and LncBase Predicted v.2 were utilized to investigate the association between lncRNA and miRNAs after validating the significant miRNAs. We estimated the expression levels of identified miRNAs and lncRNAs in BLCA and normal tissues using the wilcox.test method. Additionally, GEPIA was utilized to present the KM curve of the predicted lncRNA. Pathway enrichment comparison was conducted using Gene Set Enrichment Analysis (GSEA) to assess the differences between expression groups of the central CDIs, which were categorized based on the median.

2.7. Immunohistochemistry

Paraffin sections were prepared from samples obtained from 100 patients. The chips underwent dewaxing, antigen retrieval, endogenous peroxidase blocking, primary and secondary antibody incubation, staining, dehydration, mounting, and air drying. Antibody CHMP4C (proteintech, 1:200), E-cadherin (Fuzhou Maixin Biotechw, 1:200) and N-cadherin (Fuzhou Maixin Biotech, 1:200) were further used for immunohistochemistry. The antibody score was calculated by multiplying the staining intensity with percentages that were statistically scored using the quartile method.

2.8. Cell culture, Western blot and transwell assay

The 5637 cell line (sunncell, SKU: SNL-036, human) was cultured in RPMI-1640 medium with 10 % fetal bovine serum and 1 % penicillin/streptomycin solution in a thermostatic cell incubator. The cells were transfected by lentivirus (from Shanghai GENE biology). WB followed the routine steps of electrophoresis, membrane transfer, blocking, antibody incubation, and visualization. CHMP4C antibody (abcam, 1:1000), E-cadherin (proteintech, 1:1000) and N-cadherin (proteintech, 1:1000), β-Actin antibody (CST, 1:1000) and second antibody Rabbit (Absin, 1:2000) were used for Western Blot.

Lentivirus-transfected cells were seeded in chambers on 24-well plates at a density of 50,000 cells per well. The upper chamber was filled with 200 μL of 1640 medium, while the lower chamber contained 500 μL of 10 % fetal bovine serum. The plates were incubated in a cell incubator for 24 h. Subsequently, the chambers were fixed with 4 % paraformaldehyde and stained with crystal violet. After drying, the cells on the outer surface of the chamber were counted under a microscope.

2.9. Statistical analysis

R software version v4.0.3 was utilized for all operations conducted with the R package. The information utilized in this research was acquired from publicly accessible databases and is available for download in its original form from these resources. The data used were standardized TPM, which showed a distribution similar to the normal distribution. Hence, both the *t*-test and log-rank test could be used to assess the disparities between the two groups. Data sets were processed without randomization. Levels of significance are indicated by asterisks (*$p < 0.05$, **$p < 0.01$, ***$p < 0.001$).

3. Results

3.1. Screening and functional analysis of 763 CDIs were conducted

Initially, we compared the mRNA expression levels of these 763 CDIs in BLCA samples and normal samples obtained from the TCGA database. The heat map in Fig. 2A and the volcano plot in Fig. 2B showcased the 92 DEGs. According to the KEGG pathway analysis, these DEGs were mainly involved in Endometrial cancer, the ErbB signaling pathway, and Chronic myeloid leukemia (as depicted in Fig. 2C). The analysis of gene ontology biological process (BP) revealed that the CDIs were primarily associated with the intrinsic apoptotic signaling pathway triggered by DNA damage, the promotion of autophagy, and the control of cysteine-type endopeptidase activity (Fig. 2D). GO cellular component (CC) analysis revealed that CDIs were significant correlated to multivesicular body, plasma

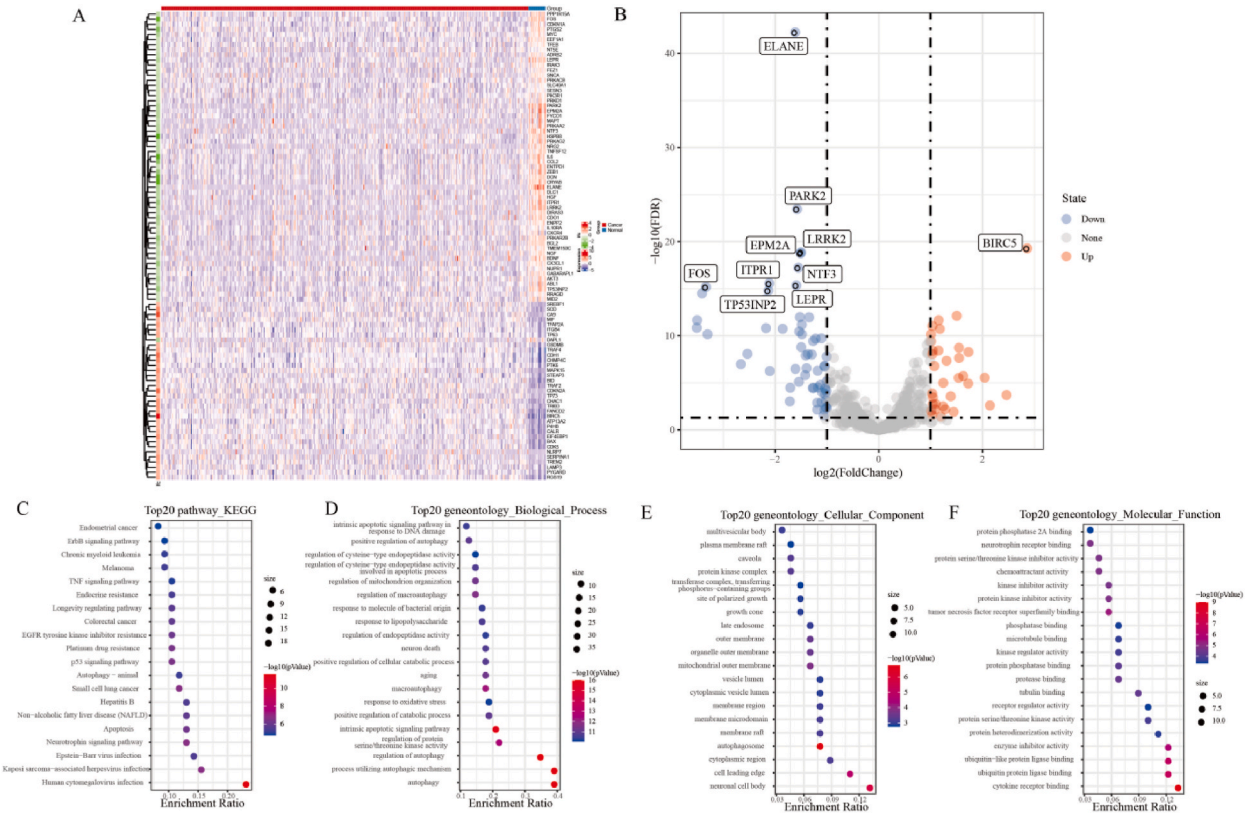

Fig. 2. Screening and functional analysis of DEGs. (A) The heatmap displays the 92 target genes that are differentially expressed. **(B)** Display a map of volcanoes representing the top 10 genes that are expressed differentially. KEGG pathway **(C)**, BP **(D)**, CC **(E)** and MF analysis (F) were performed to exhibit the top 20 relevant pathways based on the DEGs.

membrane raft and caveola (Fig. 2E). The analysis of GO Molecular function (MF) was conducted to demonstrate the CDIs primarily associated with the binding of protein phosphatase 2A, binding of neurotrophin receptors, and inhibitory activity of protein serine/threonine kinases (Fig. 2F).

3.2. Screening the 12 prognostic CDIs

To explore whether CDIs affected the prognosis of BLCA, forest plots (Fig. 3A) and KM survival analysis (Fig. 3B) were conducted. The results showed that only 12 CDIs had statistical significance. The poor prognosis in BLCA patients was found to be correlated with elevated levels of CRYAB, HSPB8, DCN, NGF, TRIB3, MYC, TFAP2A, DAPLA, and TREM2. Additionally, the low expression levels of NTF3, CHMP4C and GSDMB were also associated with poor prognosis in BLCA patients. Nevertheless, it was discovered that individuals exhibiting increased expression of CHMP4C and GSDMB had a more favorable prognosis than initially anticipated.

3.3. Subtypes analysis of the 12 CDIs

First, we used a Venn diagram to illustrate the relationship between these 12 CDIs and 13 death modes. As depicted in the figure, the key CDIs were associated with autophagy, pyroptosis, ferroptosis, and necroptosis (Fig. 4A). Furthermore, we conducted a correlation analysis among these 12 genes and identified that CRYAB and DCN as having the highest correlation coefficient (Fig. 4B).

To further study the relationship between these 12 key genes and BLCA, we conducted a subgroup analysis to divide genes into CDI-low and CDI-high subtype. Based on the optimal result, we determined that K = 2 (Fig. 4C and D). Furthermore, a heatmap was employed to exhibit the levels of expression for the 12 CDIs in both CDI-low and CDI-high subtypes (Fig. 4E). In conclusion, we assessed the influence of these two categories on the outlook of BLCA patients. Fig. 4F displayed that individuals in the CDI-high subtype experienced unfavorable outcomes in terms of overall survival, progression-free survival, and disease-specific survival. Additionally, we found associations between the two subtypes with age and TNM stage in BLCA patients (Supplementary Table 2).

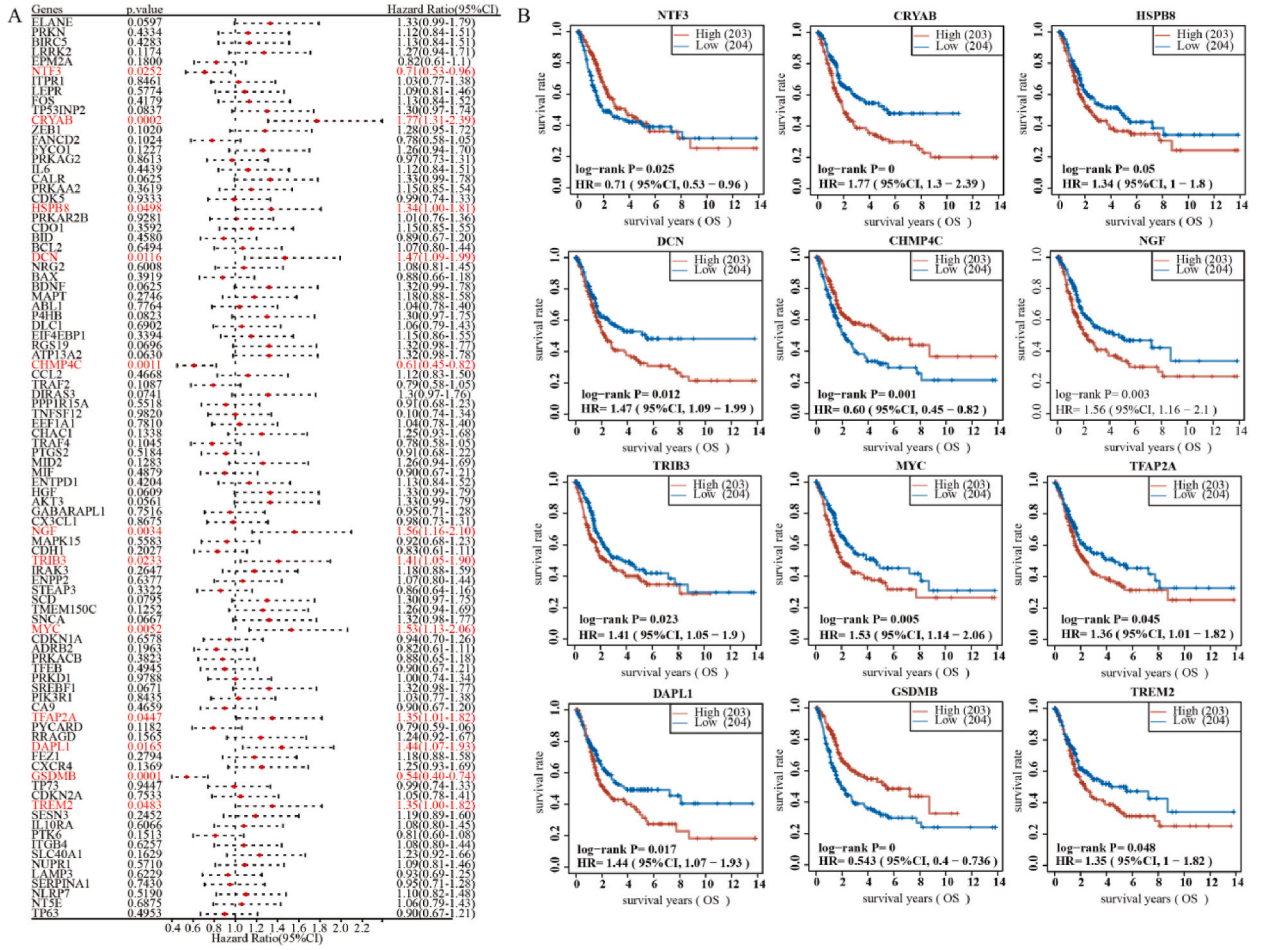

Fig. 3. Screening of the prognostic genes. (A) Prognostic forest map of 92 identified genes. (B) KM curves of 12 prognostic significantly CDIs.

3.4. DEGs, functional and mutation analysis in the subgroups

We analyzed the differential gene expression between CDI-low and CDI-high subtype, and found that 929 genes were up-regulated while 424 genes were down-regulated. The results were presented in the volcano plot (Fig. 5A). Additionally, we utilized a heat map to illustrate the relationship between these two subgroups and clinical samples (Fig. 5B). The bubble chart displayed the results of 20 up-regulated and down-regulated KEGG pathways, as well as GO analysis (Fig. 5C–F). The mutation analysis results showed that these 10 genes (TP53, TTN, KMT2D, MUC16, RB1, ARID1A, PIK3CA, KDM6A, KMT2C and EP300) have the highest mutation rate among CDI-high subtype (Fig. 6A), while these 10 genes (TTN, TP53, KDM6A, MUC16, KMT2D, ARID1A, FGFR3, SYNE1, PIK3CA and HMCN1) have the highest mutation rate among CDI-low subtype (Fig. 6B). These results indicate that TP53 and TTN may be of great significance in inducing tumor cell death.

3.5. The relationship between the subtypes and immune infiltration

Initially, we employed the 'xCell' technique to distinguish two subsets of CDIs that exhibited a correlation with 24 distinct categories of immune cells (Fig. 7A). Furthermore, employing the 'CIBERSORT' technique, we discovered that CDIs were associated with a diverse range of 15 immune cell types (as depicted in Fig. 7B). Moreover, through the utilization of the 'Timer' technique, we linked the subcategories of CDIs with T lymphocyte $CD4^{+}$, T lymphocyte $CD8^{+}$, Neutrophil, Macrophage, and Myeloid dendritic cell (Fig. 7C). Furthermore, a connection was discovered between the subcategories of CDIs and eight immune checkpoint molecules, namely CD274, CTLA4, HAVCR2, LAG3, PDCD1, PDCD1LG2, TIGIT, and SIGLEC15 (as shown in Fig. 7D). Using the TIDE score, the response of the two subtypes to an inhibitor that targets the anticipated immune checkpoint was predicted. The results showed that patients in the CDI-high subtype had poor immunotherapeutic efficacy and shorter survival after ICB treatment (Fig. 7E). Furthermore, individuals in the CDI-high subtype exhibited decreased tumor stemness scores, suggesting a decline in cellular stemness among this cohort (Fig. 7F).

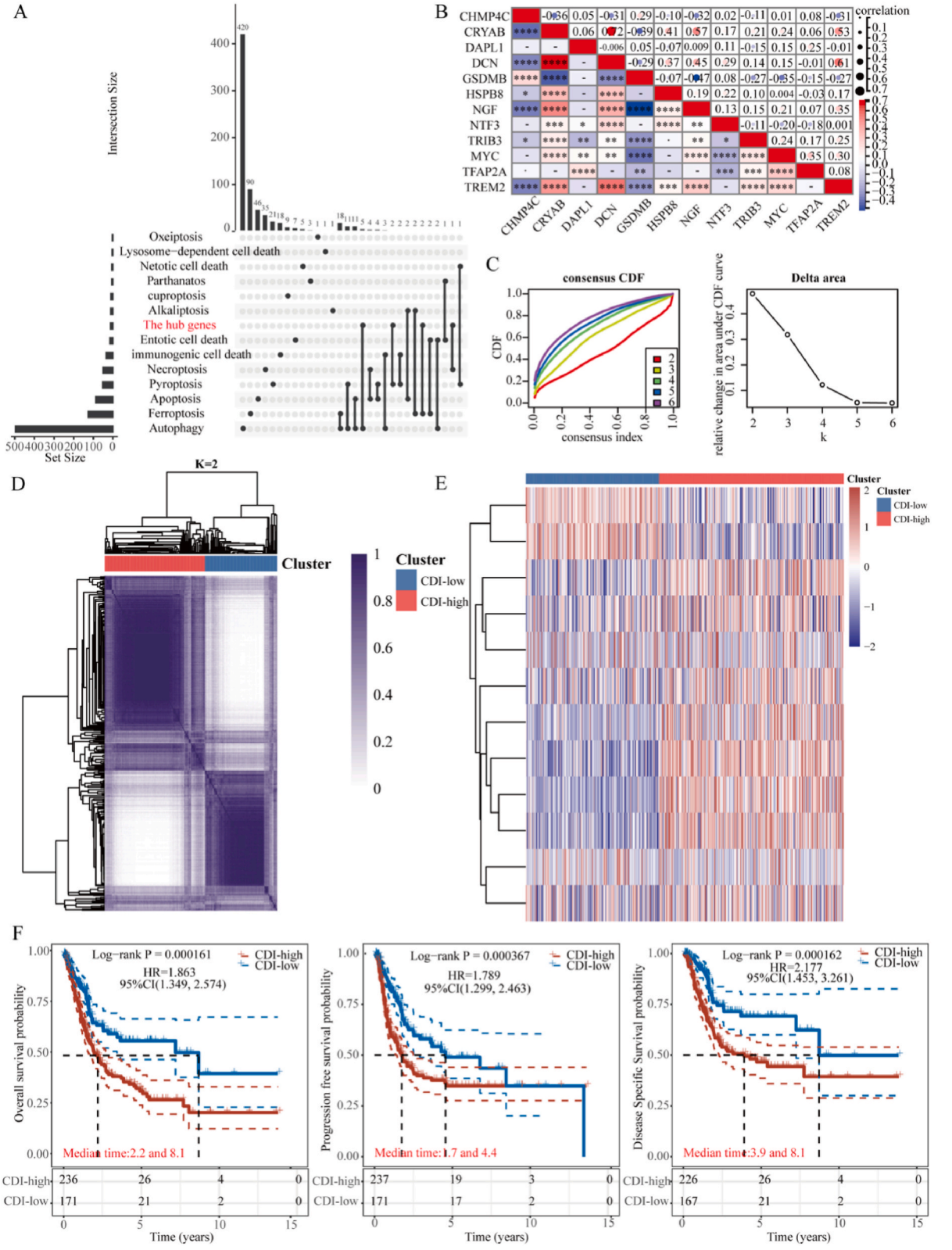

(caption on next page)

Fig. 4. Analysis of subtypes for the prognostic CDIs. (A) Venn diagram of the 13 death genes. **(B)** Correlation analysis of 12 prognostic CDIs. **(C)** The cumulative distribution function (CDF) of consensus clustering and the relative change in the area under the curve of the CDF (CDF Delta area). **(D)** Consistency of clustering results heatmap (k = 2), rows and columns represented samples, the different colors represent different types. **(E)** The expression levels of 12 CDIs in various subgroups were visualized using a heatmap, where high expression was indicated by the color red and low expression was indicated by the color blue. **(F)** The survival rates, rates of progression-free survival, and rates of survival specific to the disease for the two subcategories.

3.6. Construction of the new CDI-related prognostic model

The LASSO method was used to reduce dimensionality and construct a prognosis model based on the 12 prognostic genes mentioned above (Fig. 8A and B). The risk score was categorized into high-risk and low-risk groups based on the median value. Patients in the high-risk group had decreased survival rates and adverse outcomes compared to those in the low-risk group (Fig. 8C). We examined the correlation between the risk model and prognosis of BLCA patients using this risk model group as a basis. It was found that individuals with an increased risk experienced an unfavorable prognosis (Fig. 8D, $P < 0.001$; HR = 2.092; 95 % CI, 1.54–2.843; Median time = 1.8 years in H vs. 6.5 years in L). ROC curves were generated to predict prognostic significance at one-year, three-year, and five-year intervals with corresponding AUC values of 0.694, 0.681, and 0.702 (Fig. 8E).

3.7. Establishment of a predictive nomogram

We selected CHMP4C and GSDMB as our research targets based on their weight in the prognostic model formula. Through univariate analysis, we assessed the impact of CHMP4C, GSDMB, age, gender, T stage, TNM stage and grade on the prognosis of BLCA patients (Supplementary Fig. 1A). The findings of our study indicated that CHMP4C, GSDMB, patient age, tumor stage (T stage), and TNM stage were correlated with an unfavorable prognosis among individuals with BLCA). Based on the multivariate analyses (Supplementary Fig. 1B), GSDMB, age, and TNM stage were identified as independent factors contributing to unfavorable prognosis in BLCA patients. The predictive nomogram suggested that the model including GSDMB can estimate survival rates for 1, 3, and 5 years (Supplementary Fig. 1C), while presenting a calibration curve for the diagram (Supplementary Fig. 1D).

3.8. Relevance of the hub CDIs and immunity

Firstly, we investigated whether the presence of the 2 CDIs in BLCA contributes to immune cell infiltration. In addition, we examined the correlation between these two CDIs and the tumor immune microenvironment (TIME). To demonstrate their strong association with immunity in BLCA, we utilized ImmuneScore, StromalScore, and ESTIMATEScore (Fig. 9A–C).

The evaluation of the correlation between central hub CDIs and immune checkpoints involved the utilization of CD274, CTLA4, HAVCR2, LAG3, PDCD1, PDCD1LG2, TIGIT, and SIGLEC15. The results indicate a significant correlation between the expression of CHMP4C or GSDMB and immune checkpoints. The low expression group of CHMP4C exhibited higher levels of immune checkpoints (CD274, CTLA4, HAVCR2, LAG3, PDCD1, PDCD1LG2, and TIGIT) compared to the high expression group. However, SIGLEC15 showed the opposite trend in both groups. The comparison also included a normal group of patients (Fig. 9D). Furthermore, the normal group exhibited no notable disparity in the expression of GSDMB and PDCD1 (Fig. 9E). The low expression of CDIs in the hub, as shown previously, indicated a poor prognosis. It was hypothesized that the group with decreased expression had a higher presence of immune checkpoint molecules, enabling the tumor to evade the immune system. Subsequently, we utilized the TIDE algorithm to evaluate the impact of ICB on both groups. The findings revealed that the group with lower expression levels exhibited a greater TIDE score for CHMP4C and GSDMB, suggesting a reduced survival duration following ICB therapy compared to the group with higher expression levels (Fig. 9F and G). The outcome aligns with our earlier deduction.

3.9. Building of the regulatory network for CHMP4C and GSDMB

In order to gain a deeper understanding of the hub CDIs in BLCA, we created a network that showcases the interactions between lncRNA and microRNA. By searching the databases miRTarBase and Tarbase v8, we found one miRNA targeting CHMP4C and two miRNAs targeting GSDMB in miRTarBase. In Tarbase v8, we found 11 miRNAs targeting CHMP4C and 16 miRNAs targeting GSDMB. After merging the two aforementioned databases and intersecting the related microRNAs for both CDIs, we finally identified two regulatory microRNAs for both CHMP4C and GSDMB: miR-146a-5p and miR-429 (Fig. 10A). Next, we evaluated the expression levels of these two microRNAs in BLCA samples from TCGA database as well as normal samples. The data showed high expression levels of both microRNAs in BLCA (Fig. 10B and C).

In lncBase Predicted v2, we identified 672 lncRNAs interacting with miR-146a-5p and 538 lncRNAs interacting with miR-429. In StarBase v2, we found 37 lncRNAs interacting with miR-146a-5p and 28 lncRNAs interacting with miR-429. After intersecting the four datasets, we obtained the lncRNAs XIST and NEAT1 (Fig. 10D). The levels of XIST and NEAT1 were evaluated, revealing a significant disparity between the BLCA and control cohorts (including TCGA and 40 GTEx data) (as depicted in Fig. 10E and F). Furthermore, NEAT1 exhibited prognostic value for BLCA (Fig. 10G). Additionally, we explored potential pathways involved in the hub CDIs of BLCA through GSEA. Consequently, we found a significant association between the epithelial-mesenchymal transition (EMT) pathway and

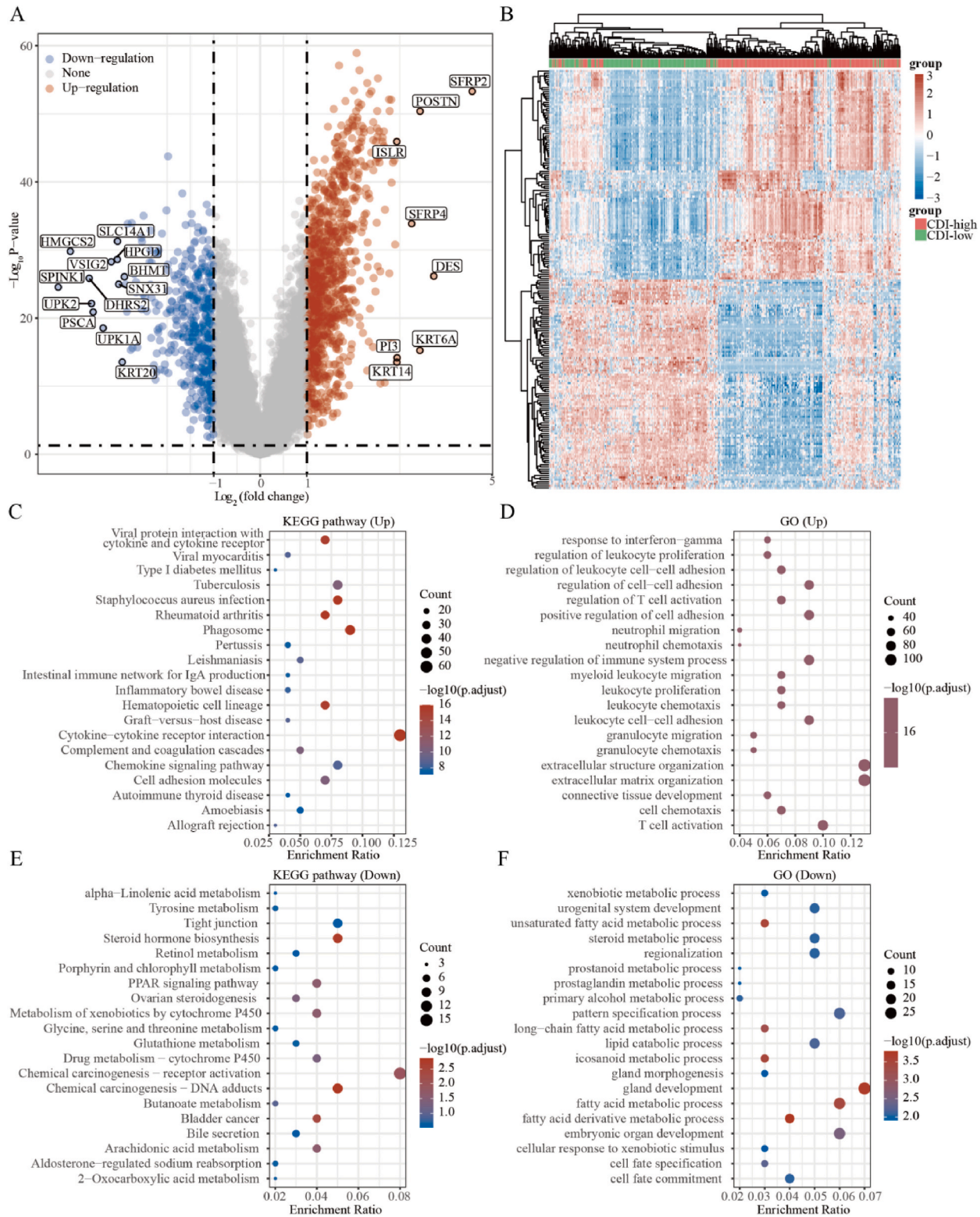

Fig. 5. DEGs analysis of the subtypes. **(A)** Volcano map to show the DEGs for the subtypes. **(B)** The heatmap to show the DEGs for the subtypes. **(C)** KEGG pathway to show the top 20 up pathways. **(D)** GO analysis to show the top 20 up pathways. **(E)** KEGG pathway to show the top 20 down pathways. **(F)** GO analysis to show the top 20 down pathways.

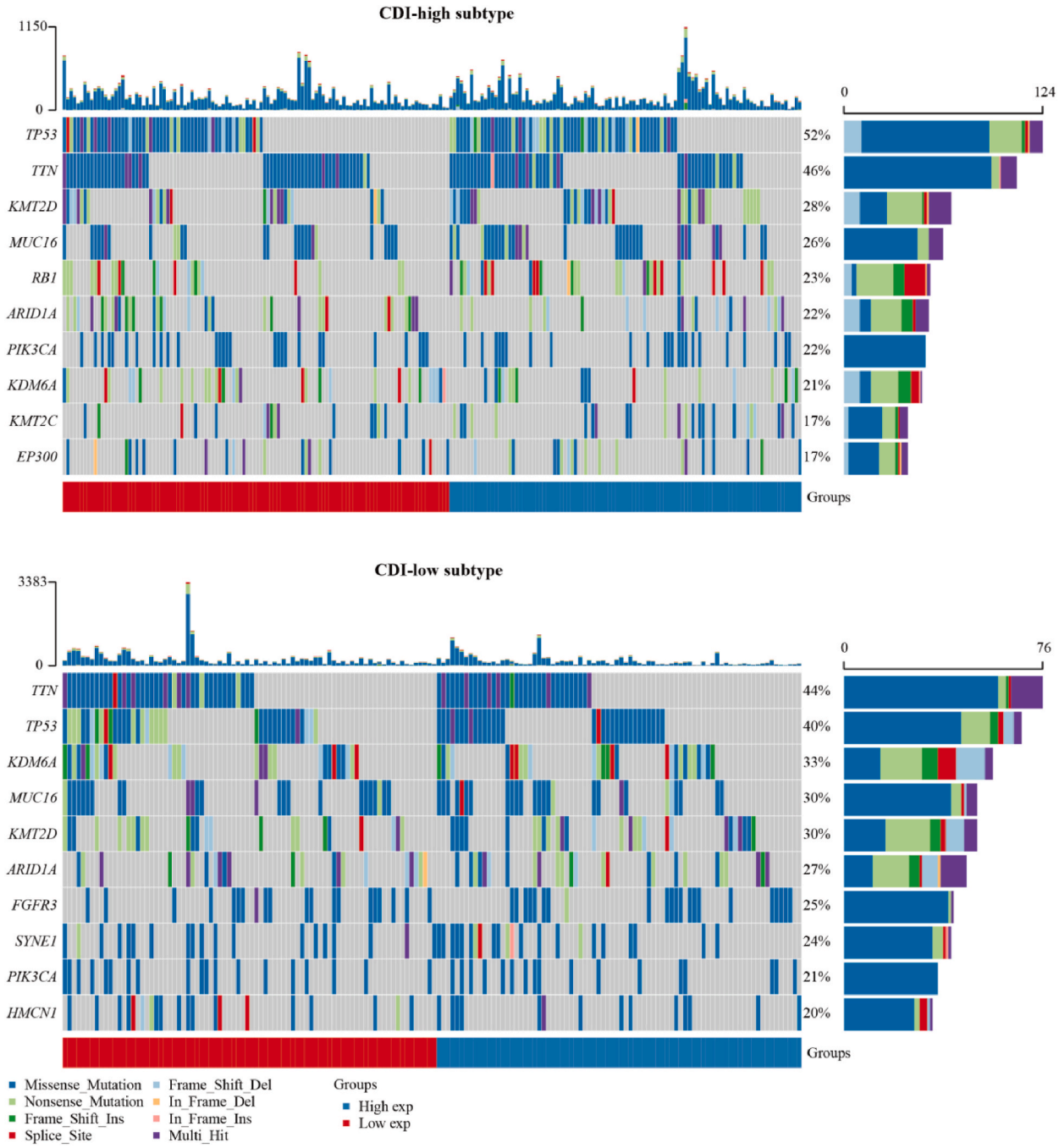

Fig. 6. The mutations between two subtypes. (A, B) Genetic mutation landscape waterfall map to exhibit the top 10 mutation genes in the CDI-high/low subtype.

the CDIs (Fig. 10H and I). Therefore, our speculation is that low expression of CHMP4C and GSDMB may impact tumor metastasis process and prognosis in patients.

3.10. CHMP4C is involved in the EMT pathway in BLCA by experiments

According to the TCGA database, CHMP4C exhibited significantly elevated expression levels in BLCA tissues (Fig. 11A). Consistently, our center's data also supported this conclusion (Fig. 11B). To further elucidate the potential oncogenic mechanism of CHMP4C, we conducted a bioinformatics analysis and identified a potential association between CHMP4C and the EMT pathway

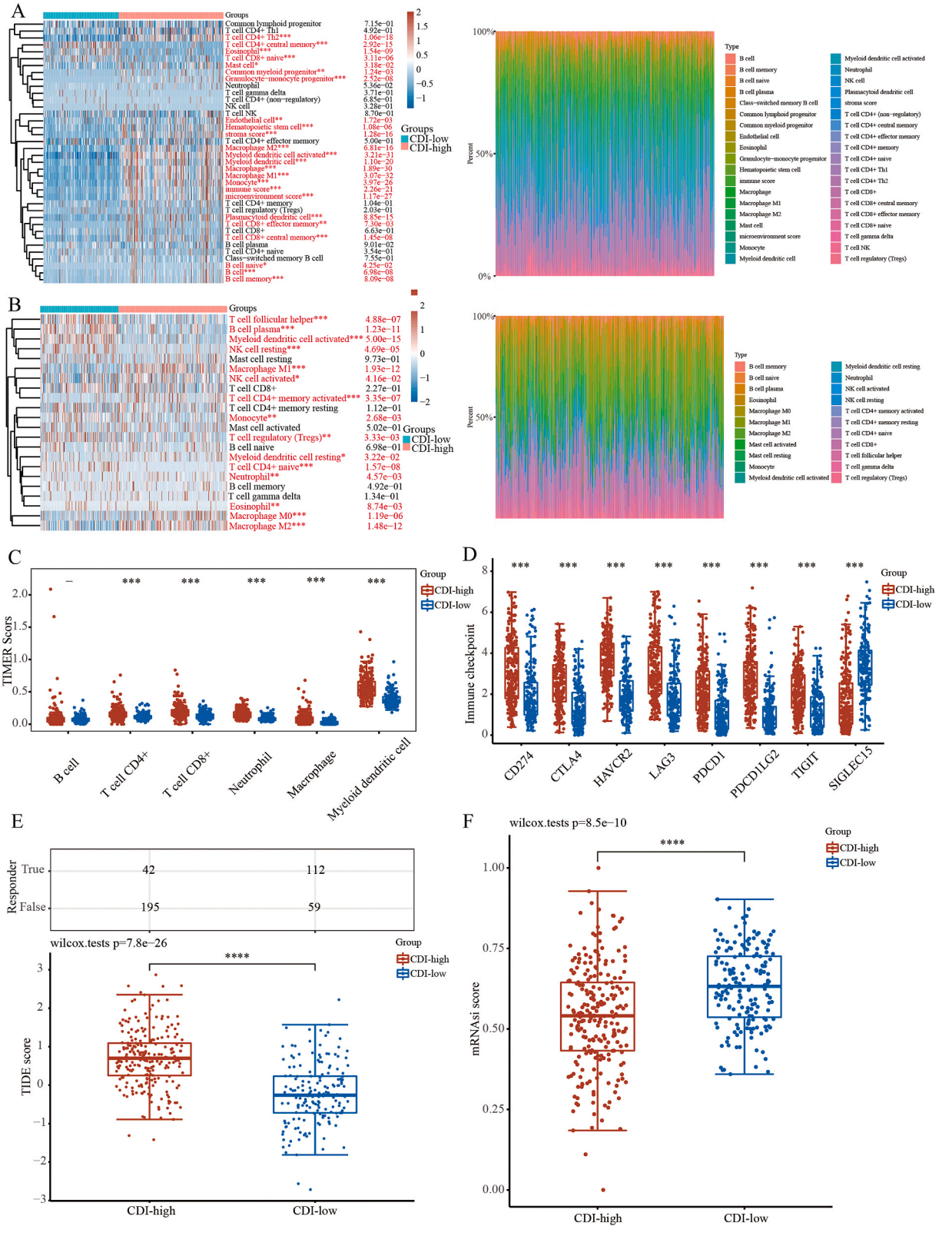

(caption on next page)

Fig. 7. Immunotherapy of the two subtypes. (A) Utilizing the 'xCell' tool, we can examine the association between the two subsets of CDIs and the diverse range of 24 immune cell categories. **(B)** Using the method of 'CIBERSORT', we examined the relationship between the two subcategories of CDIs and the 15 distinct categories of immune cells. **(C)** The correlation between the two subgroups of CDIs and the 6 distinct categories of immune cells will be analyzed using the 'TIMER' tool. **(D)** The correlation between the two subgroups of CDIs and the 8 different immune checkpoint genes. **(E)** TIDE score to show the immunotherapy efficacy between the two subgroups. **(F)** mRNAsi score to show the tumor stemness between the two subgroups.

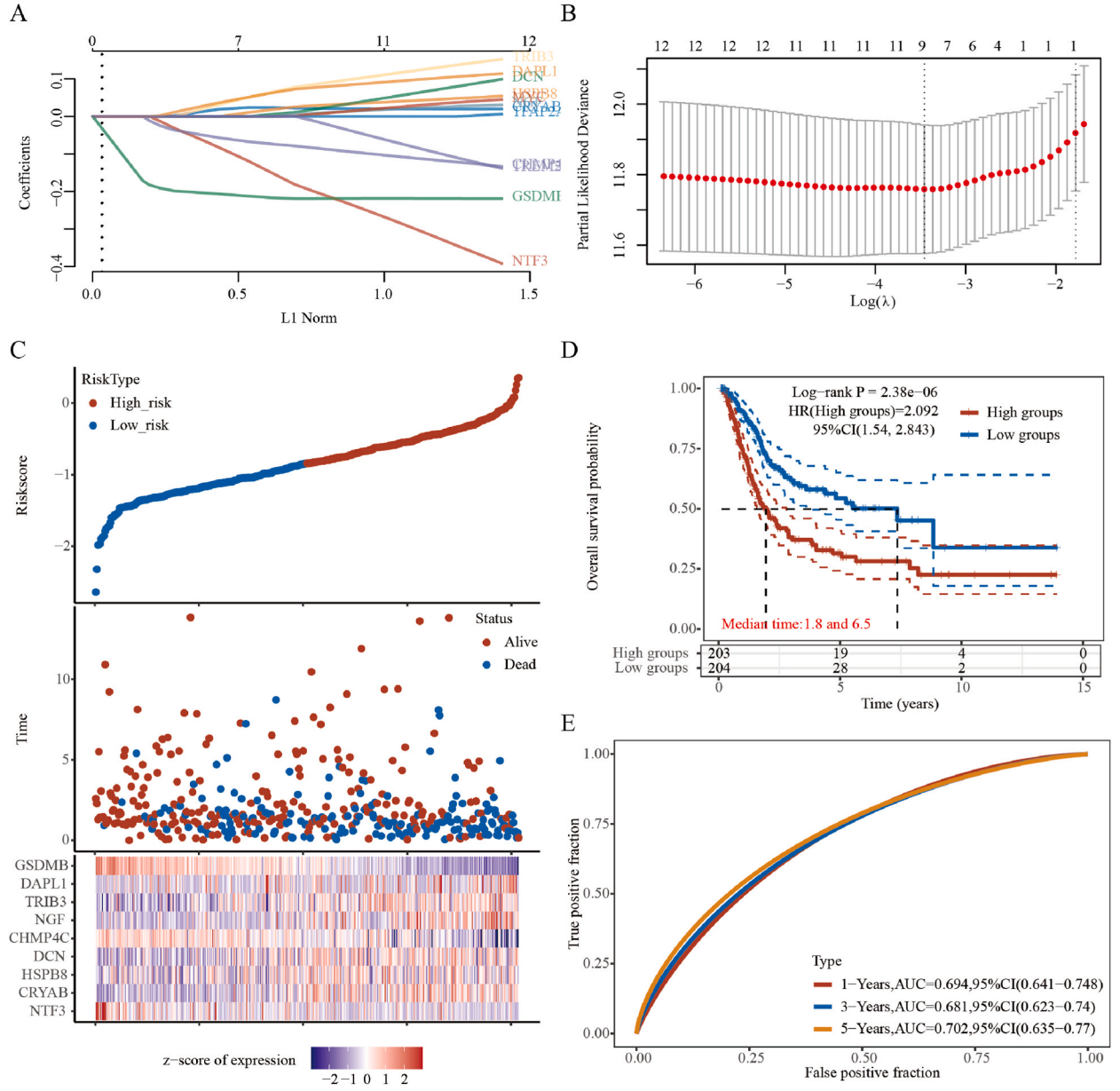

Fig. 8. Establishment and evaluation of a prognostic risk model. (A) Lasso regression model to establish prognostic model. **(B)** Plots of the ten-fold cross-validation error rates. **(C)** Information grouping by the risk score, the survival status, and the expression of PRGs shown by heatmap in BLCA. **(D)** Prognostic overall survival curve of risk model. **(E)** ROC curve to measure the 1,3,5-years predictive value of prognostic model in BLCA.

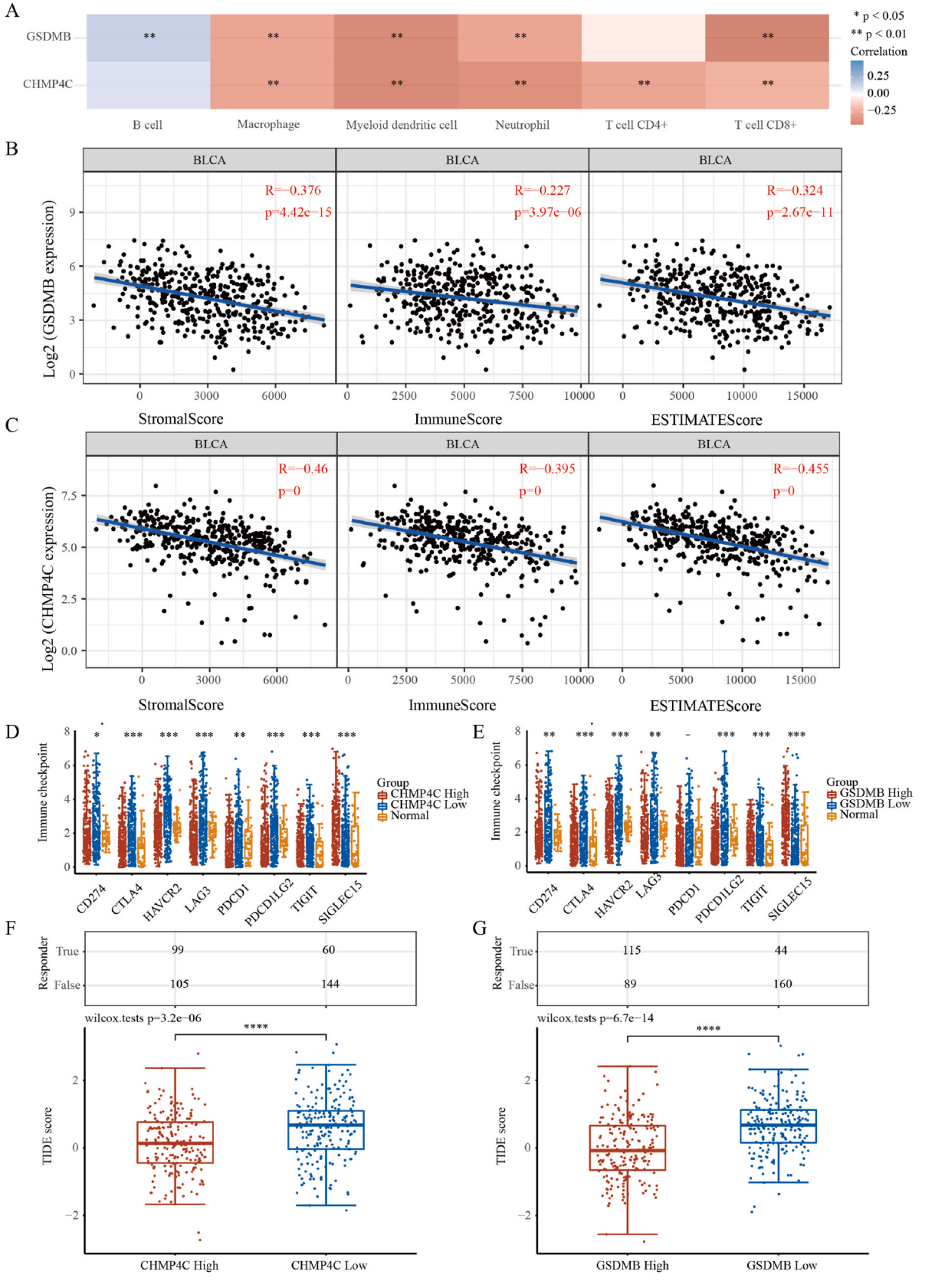

(caption on next page)

Fig. 9. The analysis of immunotherapy for the two hub genes. (A) The Spearman correlation between the 2 hub genes and 6 immune cells. **(B, C)** The spearman correlation between the 2 genes and the tumor immune microenvironment (ImmuneScore, StromalScore and ESTIMATEScore). **(D, E)** The relationship between the expression of the two genes and eight immune checkpoint genes in BLCA. **(F, G)** The prediction results include a statistical table showing the immune response of samples (above) and the distribution of immune response scores (below) in various groups.

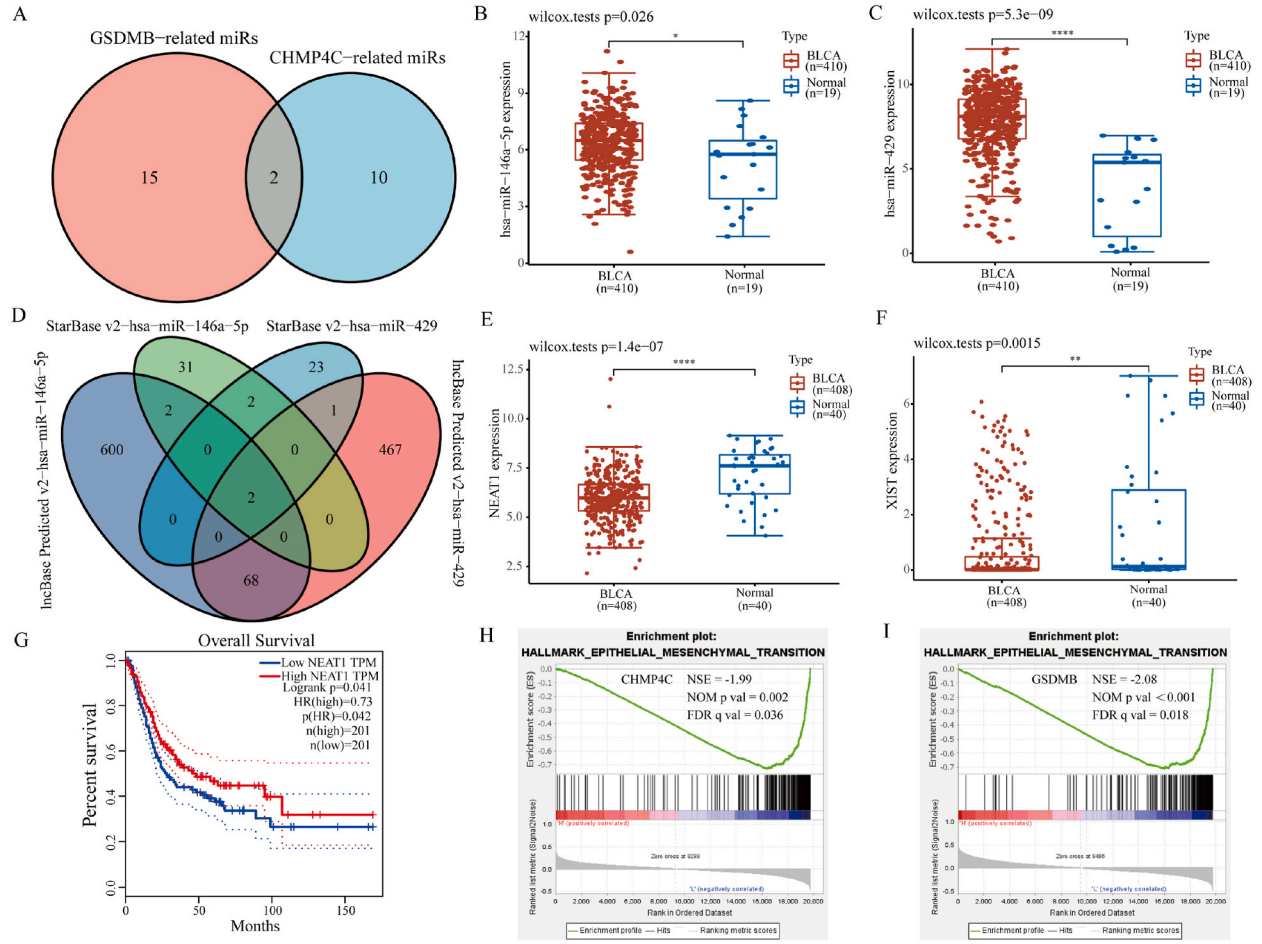

Fig. 10. Construction of regulation network for the hub CDIs. (A) The Venn for related miRNAs for CHMP4C and GSDMB from mirTarBase and TarBase V.8. **(B, C)** The expression of identified miRNAs such as miR-146a-5p and miR-429 in BLCA and normal samples. **(D)** The Venn diagram illustrates the overlap between lncRNAs identified by miRNAs from lncBase predicted V.2 and StarBase V2.0. **(E, F)** The expression of identified lncRNAs such as lncRNA XIST and NEAT1 in BLCA and normal samples. **(G)** The OS of lncRNA NEAT1 in the high vs low expression group in BLCA. **(H, I)** GSEA for the low expression group of CHMP4C and GSDMB.

(Fig. 11C). Fig. 11D and E demonstrated a direct association between the expression of CHMP4C and the levels of N-Cadherin, while an inverse relationship was observed with the expression of E-Cadherin, as indicated by immunohistochemical analysis. CHMP4C induced changes in the expression of EMT-related genes at the cellular level (Fig. 11F), which were consistent with the immunohistochemical results. Additionally, CHMP4C promoted the metastasis of BLCA cells. (Fig. 11G). In conclusion, CHMP4C is involved in influencing BLCA through the EMT pathway.

4. Discussion

Previous studies on tumor cell death did not indicate the dominant mode [20–22]. In this manuscript, we propose that pyroptosis plays a crucial role in BLCA among all modes of cell death. Previous research has shown the significant involvement of pyroptosis in BLCA [23,24]. We identified CHMP4C and GSDMB as key factors, particularly GSDMB, which exhibited abnormal up-regulation leading to enhanced growth and invasion of BLCA cells [25]. GSDMB has been implicated in tumor progression and metastasis [26, 27]. Phosphorylation of CHMP4C can inhibit apoptosis, while its depletion enhances radiation sensitivity and prolongs the S phase of the cell cycle in lung cancer [28]. Overexpression of CHMP4C was associated with lower survival rates in cervical cancer. In contrast to

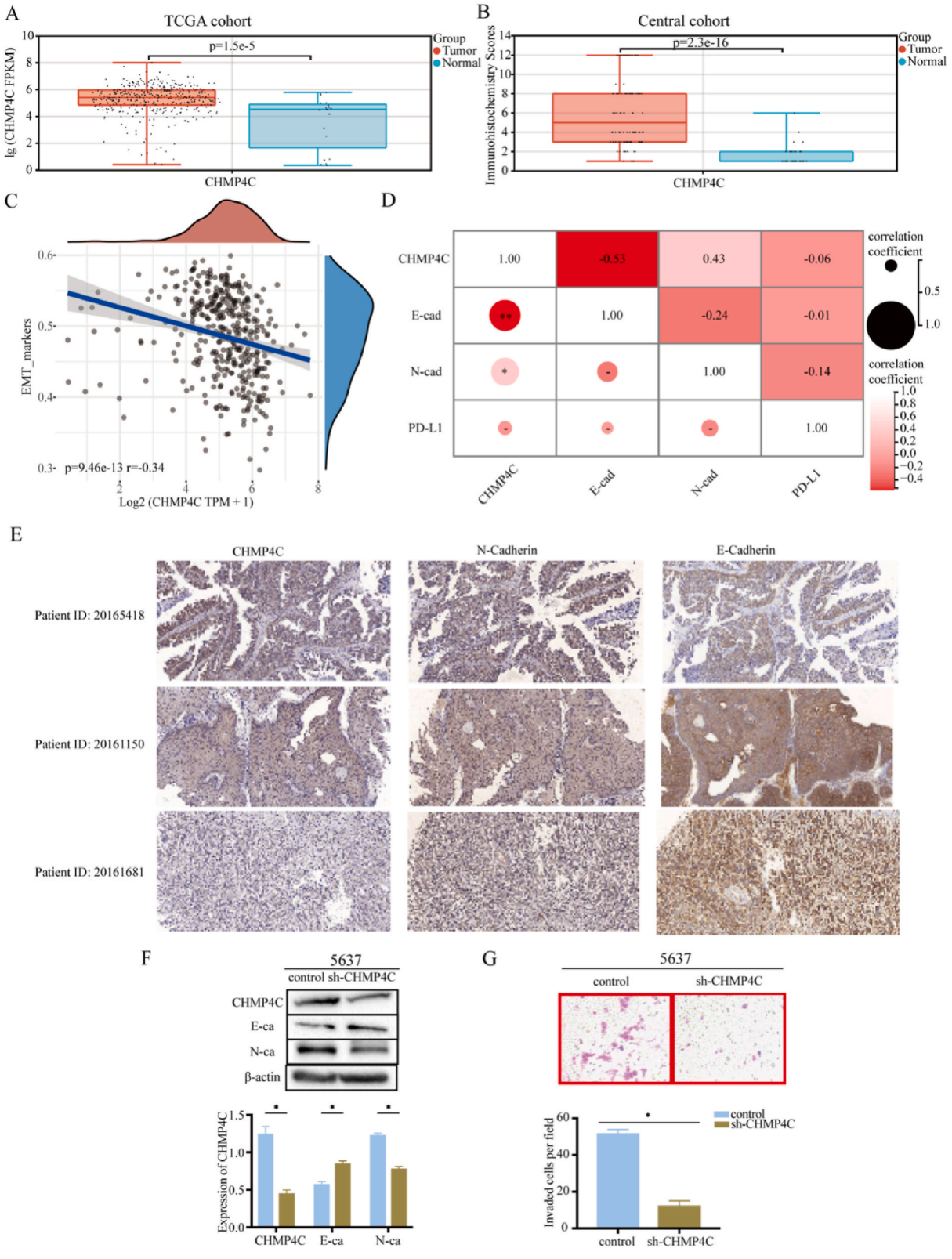

(caption on next page)

Fig. 11. The expression and function of CHMP4C. (A) The expression of CHMP4C in bladder tumor (n = 408) and normal (n = 19) tissues in TCGA. **(B)** The expression of CHMP4C in bladder tumor (n = 100) and normal (n = 39) tissues in our central cohort. **(C)** The correlation between CHMP4C and EMT_markers in TCGA. **(D)** The correlation between CHMP4C and related-EMT_markers in our central cohort. **(E)** The typical immunohistochemical image for CHMP4C, N-Cadherin and E-Cadherin. **(F)** Western blot showed the effect of CHMP4C on the expression of N-Cadherin and E-Cadherin. **(G)** Transwell assay revealed the migratory capacity of cells with CHMP4C knockdown.

what we expected, the increase in CHMP4C expression in c-33a cells may enhance both cell proliferation and metastasis [29]. However, the unique roles of CHMP4C and GSDMB in BLCA have not been previously reported.

It appeared that the expression of CHMP4C and GSDMB in BLCA was inconsistent with prognosis, which contradicted the predominant prognostic model. Of the 2 CDIs involved in tumors, overexpression of CHMP4C represents a worse prognosis for cervical cancer [29]. The expression of GSDMB was a poor prognostic factor for HER2 positive breast cancer [30]. The results were the opposite in BLCA, which was consistent with CXCL11 expression in colon adenocarcinoma [31]. To investigate the reason why low expression of CHMP4C and GSDMB led to a worse prognosis, we first examined their immune relevance. We found that infiltrating lymphocytes were independent prognostic factors for tumors [32,33]. Therefore, the correlation between CDIs and infiltrating immune cells suggests that CDIs may participate in tumor immunity processes and affect BLCA prognosis. Moreover, the correlation between CDIs and immunity was explored by utilizing immune score and matrix score. Under normal circumstances, immune checkpoint molecules serve as safeguards against excessive autoimmunity; however, they can also facilitate tumor immune evasion in abnormal situations. For CHMP4C and GSDMB, we analyzed the differential expression of immune checkpoint molecules in the high expression group, low expression group, and normal bladder sample group. The discovery revealed that the low expression groups of the two CDIs exhibited increased immune-related enrichment, suggesting enhanced immune evasion by the tumor and consequently leading to its progression. The outcome aligns with the forecast stated for CHMP4C and GSDMB.

In order to prove the above point, CHMP4C was selected for further study. In this study, the immunohistochemical expression of CHMP4C was validated, and its correlation with EMT was examined. The expression of CHMP4C was consistent with the results of bioinformatics analysis, which aligned with the performance of CHMP4C in cervical cancer [29]. To our surprise, patients with high CHMP4C expression had a worse prognosis (Supplementary Table 3), which was contrary to the predicted results. We attribute these unpredictable outcomes to the complex regulation of RNA-to-protein translation during tumorigenesis and progression. Previous studies have shown that EMT is associated with the activation of different immune checkpoint molecules, including PD-L1 [34]. EMT-induced immune evasion promotes cancer progression. Additionally, our study suggested that CHMP4C may influence EMT alterations. It is well established that EMT is closely linked to tumor metastasis. However, based on the collected clinical data, CHMP4C is not closely related to tumor metastasis (perhaps due to our insufficient sample size, Supplementary Table 4). Therefore, we hypothesize that CHMP4C promotes the progression of BLCA by affecting the immune evasion through the EMT pathway.

In conclusion, we screened core genes from the perspective of CDIs and focused on exploring the relationship between hub CDIs and immunity in BLCA. As a result, we found that the CDIs were highly correlated with immune checkpoints, providing insights into ICB treatment. Furthermore, the establishment of a regulatory network has helped us to understand the specific role of CDIs in BLCA. The limitation of this article is the failure to investigate how CHMP4C influences immunity through EMT at the cellular level. Because the patients involved in this study had relatively low PD-L1 expression, the relationship between CHMP4C and immunity was not well elucidated. Additionally, more verification at the animal level is required to determine the effect of CHMP4C on immunotherapy. Finally, we will continue to collect data from patients with bladder cancer treated with immunotherapy (for example: PD-L1 expression or corresponding inhibitor treatment effect) in the future to verify our conclusions.

5. Conclusions

By analyzing 13 pathways, we identified two central genes (CHMP4C and GSDMB) to investigate the disparity in expression between tumor and normal tissues, and assess their influence on the prognosis of BLCA. A prognostic model was constructed using these two genes, which were found to be involved in predicting the prognosis of BLCA. Furthermore, it was explained that these hub genes are related to immune infiltration and immunotherapy. Finally, the regulatory network of these two genes was constructed. The immunohistochemistry and cell experiment results demonstrated that CHMP4C influences the development of BLCA through the EMT pathway. In summary, the current findings emphasize the harmful impact of CHMP4C and GSDMB on the outlook of BLCA individuals, presenting a chance to enhance the response to immunotherapy.

Ethics approval and consent to participate

This study has been approved by Nantong Tumor Hosptial Medical Ethics Committee (No.2023- A 13) on December 1, 2023. The written informed consent was obtained from the patients for the use of their tissues in research.

Consent for publication

Not applicable.

Availability of data and materials

Most of the data are available from public databases, and there are links in the corresponding places of the article (Materials and methods - Selection and application of database). Besides, our central data generated involved in the research are available from the corresponding author on reasonable request.

Funding

This research was funded by the Nantong Commission of Health (MSZ2023036). The funding provided by the organization has contributed to the completion of this study, including the coverage of publishing costs for this article.

CRediT authorship contribution statement

Mingde Gao: Writing – original draft, Software, Methodology, Funding acquisition, Formal analysis. **Haifeng Guo:** Validation, Data curation. **Haifei Xu:** Validation, Supervision, Conceptualization. **Xiaoxia Jin:** Formal analysis. **Yushan Liu:** Formal analysis. **Zhigang Chen:** Project administration. **Xiaolin Wang:** Writing – review & editing, Project administration, Conceptualization.

Declaration of competing interest

The authors declare that they have no known competing financial interests or personal relationships that could have appeared to influence the work reported in this paper.

Acknowledgements

We would like to thank the researchers and participants for their contributions. Also, we would like to thank the Assistant for Clinical Bioinformatics (https://www.aclbi.com).

Appendix A. Supplementary data

Supplementary data to this article can be found online at https://doi.org/10.1016/j.heliyon.2024.e33200.

References

[1] L. Galluzzi, I. Vitale, S.A. Aaronson, et al., Molecular mechanisms of cell death: recommendations of the nomenclature committee on cell death 2018, Cell Death Differ. 25 (3) (2018) 486–541.
[2] Y. Bi, Z.H. Wu, F. Cao, Prognostic value and immune relevancy of a combined autophagy-, apoptosis- and necrosis-related gene signature in glioblastoma, BMC Cancer 22 (1) (2022) 233.
[3] W. Lin, Y. Chen, B. Wu, Y. Chen, Z. Li, Identification of the pyroptosis-related prognostic gene signature and the associated regulation axis in lung adenocarcinoma, Cell Death Dis. 7 (1) (2021) 161.
[4] G. Tu, W. Peng, Q. Cai, et al., Construction and validation of a 15-gene ferroptosis signature in lung adenocarcinoma, PeerJ 9 (2021) e11687.
[5] D. Tang, R. Kang, T.V. Berghe, P. Vandenabeele, G. Kroemer, The molecular machinery of regulated cell death, Cell Res. 29 (5) (2019) 347–364.
[6] M. Inoue, M. Enomoto, M. Yoshimura, T. Mizowaki, Pharmacological inhibition of sodium-calcium exchange activates NADPH oxidase and induces infection-independent NETotic cell death, Redox Biol. 43 (2021) 101983.
[7] X. Wang, S. Wu, F. Liu, et al., An immunogenic cell death-related classification predicts prognosis and response to immunotherapy in head and neck squamous cell carcinoma, Front. Immunol. 12 (2021) 781466.
[8] J. Liu, F. Kuang, R. Kang, D. Tang, Alkaliptosis: a new weapon for cancer therapy, Cancer Gene Ther. 27 (5) (2020) 267–269.
[9] X. Fang, E. Dai, L. Bai, et al., The HMGB1-AGER-STING1 pathway mediates the sterile inflammatory response to alkaliptosis, Biochem. Biophys. Res. Commun. 560 (2021) 165–171.
[10] P. Scaturro, A. Pichlmair, Oxeiptosis-a cell death pathway to mitigate damage caused by radicals, Cell Death Differ. 25 (7) (2018) 1191–1193.
[11] C.X. Wang, L.H. Chen, H.B. Zhuang, et al., Auriculasin enhances ROS generation to regulate colorectal cancer cell apoptosis, ferroptosis, oxeiptosis, invasion and colony formation, Biochem. Biophys. Res. Commun. 587 (2022) 99–106.
[12] P. Scaturro, A. Pichlmair, Oxeiptosis: a discreet way to respond to radicals, Curr. Opin. Immunol. 56 (2019) 37–43.
[13] P. Tsvetkov, S. Coy, B. Petrova, et al., Copper induces cell death by targeting lipoylated TCA cycle proteins, Science 375 (6586) (2022) 1254–1261.
[14] F. Bray, J. Ferlay, I. Soerjomataram, R.L. Siegel, L.A. Torre, A. Jemal, Global cancer statistics 2018: GLOBOCAN estimates of incidence and mortality worldwide for 36 cancers in 185 countries, CA Cancer J Clin 68 (6) (2018) 394–424.
[15] A.T. Lenis, P.M. Lec, K. Chamie, Bladder cancer, JAMA 324 (19) (2020) 2006.
[16] L. Tran, J.F. Xiao, N. Agarwal, J.E. Duex, D. Theodorescu, Advances in bladder cancer biology and therapy, Nat. Rev. Cancer 21 (2) (2021) 104–121.
[17] J.C. Pardo, V. Ruiz de Porras, A. Plaja, et al., Moving towards personalized medicine in muscle-invasive bladder cancer: where are we now and where are we going, Int. J. Mol. Sci. 21 (17) (2020).
[18] S. Antoni, J. Ferlay, I. Soerjomataram, A. Znaor, A. Jemal, F. Bray, Bladder cancer incidence and mortality: a global overview and recent trends, Eur. Urol. 71 (1) (2017) 96–108.
[19] F. Abdollah, G. Gandaglia, R. Thuret, et al., Incidence, survival and mortality rates of stage-specific bladder cancer in United States: a trend analysis, Cancer Epidemiol 37 (3) (2013) 219–225.
[20] Y. Hong, Y. Yuan, Z.K. Liu, et al., A pan-cancer analysis of prognostic and immunological roles for cell death genes, Genes 14 (6) (2023).
[21] W. Xu, H. Tang, A. Anwaier, et al., Immunogenomic characteristics of cell-death-associated genes with prognostic implications in bladder cancer, Front. Immunol. 7 (13) (2022) 909324.

[22] L.S. Zhang, M. Peng, et al., Integrated bioinformatic analysis identified a novel prognostic pan-programmed cell death signature for bladder cancer, Front. Immunol. 1 (13) (2022) 1030097.
[23] Y. Tu, X. Ding, Z. Mao, Identification and verification of the pyroptosis-related prognostic signature and its associated regulatory axis in bladder cancer, Front. Cell Dev. Biol. 10 (2022) 912008.
[24] Y. Yan, X. Cao, Z. Wang, et al., Pyroptosis-related patterns predict tumor immune landscape and immunotherapy response in bladder cancer, Front. Mol. Biosci. 9 (2022) 815290.
[25] H. He, L. Yi, B. Zhang, et al., USP24-GSDMB complex promotes bladder cancer proliferation via activation of the STAT3 pathway, Int. J. Biol. Sci. 17 (10) (2021) 2417–2429.
[26] H. Komiyama, A. Aoki, S. Tanaka, et al., Alu-derived cis-element regulates tumorigenesis-dependent gastric expression of GASDERMIN B (GSDMB), Genes Genet. Syst. 85 (1) (2010) 75–83.
[27] M. Hergueta-Redondo, D. Sarrió, Á. Molina-Crespo, et al., Gasdermin-B promotes invasion and metastasis in breast cancer cells, PLoS One 9 (3) (2014) e90099.
[28] K. Li, J. Liu, M. Tian, et al., CHMP4C disruption sensitizes the human lung cancer cells to irradiation, Int. J. Mol. Sci. 17 (1) (2015).
[29] S.L. Lin, M. Wang, Q.Q. Cao, Q. Li, Chromatin modified protein 4C (CHMP4C) facilitates the malignant development of cervical cancer cells, FEBS Open Bio 10 (7) (2020) 1295–1303.
[30] M. Hergueta-Redondo, D. Sarrio, Á. Molina-Crespo, et al., Gasdermin B expression predicts poor clinical outcome in HER2-positive breast cancer, Oncotarget 7 (35) (2016) 56295–56308.
[31] Y. Cao, N. Jiao, T. Sun, et al., CXCL11 correlates with antitumor immunity and an improved prognosis in colon cancer, Front. Cell Dev. Biol. 9 (2021) 646252.
[32] P. Ge, W. Wang, L. Li, et al., Profiles of immune cell infiltration and immune-related genes in the tumor microenvironment of colorectal cancer, Biomed. Pharmacother. 118 (2019) 109228.
[33] R.A. de Jong, N. Leffers, H.M. Boezen, et al., Presence of tumor-infiltrating lymphocytes is an independent prognostic factor in type I and II endometrial cancer, Gynecol. Oncol. 114 (1) (2009) 105–110.
[34] Y.Y. Jiang, H.X. Zhan, et al., Communication between EMT and PD-L1 signaling: new insights into tumor immune evasion, Cancer Lett. 1 (468) (2020) 72–81.